Ultra-Broadband Interleaver for Extreme Wavelength Scaling in Silicon Photonic Links

Anthony Rizzo, *Graduate Student Member, IEEE*, Qixiang Cheng, *Member, IEEE*, Stuart Daudlin, and Keren Bergman, *Fellow, IEEE*

***Abstract*— We demonstrate an ultra-broadband silicon photonic interleaver capable of interleaving and de-interleaving frequency comb lines over a 125 nm bandwidth in the extended C- and L-bands. We use a ring-assisted asymmetric Mach Zehnder interferometer to achieve a flat-top passband response while maintaining a compact device footprint. The device has a 400 GHz free spectral range to divide an optical frequency comb with 200 GHz channel spacing into two output groups, each with a channel spacing of 400 GHz, yielding a potential capacity of 78 total wavelength-division multiplexed channels between 1525 nm and 1650 nm. This device represents an important step towards realizing highly parallel integrated optical links with broadband frequency comb sources within the silicon photonics platform.**

***Index Terms*— Silicon photonics, optical frequency combs, wavelength division multiplexing.**

I. Introduction

THE explosive growth of data-intensive applications such as machine learning and artificial intelligence has placed a great strain on interconnection bandwidths in data center and high performance computing systems. Furthermore, the COVID-19 pandemic has caused a rapid and unprecedented shift towards a digital world which requires millions of simultaneous high-definition video streams across the globe for telecommuting. This extreme bandwidth pressure has led to conservative estimates of 8% of the total global electricity being consumed by data centers alone by 2030, with current trends indicating as high as 21% is possible without significant intervention [1]. Thus, optical interconnects will become ubiquitous in the coming years due to their reduced energy consumption and large bandwidth potential [2]. In particular, silicon photonics is poised to revolutionize data center interconnects due to its extreme device density arising from the large index contrast between Si and SiO_2 and its potential to leverage the same economies of scale as the electronics industry by sharing the tremendous global investment in silicon processing through CMOS infrastructure.

A major advantage afforded by optical interconnects is the ability to send many parallel data streams through a single fiber using wavelength division multiplexing (WDM). Currently, the optical channels for WDM systems are generated by laser arrays where each laser must be individually tuned to maintain the desired channel spacing. Recent advances in microresonator-based optical frequency combs have given rise to a new paradigm for WDM sources where many wavelength channels are generated on-chip with precise, intrinsic channel spacing and correlated drift [3], [4]. Such comb sources can have bandwidths spanning hundreds of nanometers and can consist of hundreds of distinct wavelength tones. In order to utilize the full comb bandwidth, all devices on the silicon photonic chip must have a broadband design.

De-interleaving and interleaving are essential operations for spectrally separating groups of comb lines into different bus waveguides and recombining them on a single bus, respectively. Traditional approaches for silicon photonic links with frequency comb sources, which use cascaded micro-ring resonators (MRRs), have a fundamental restriction on the number of wavelength channels on a single bus due to the free spectral range (FSR) of the MRRs, insertion loss (IL) of each MRR, and crosstalk for increasingly smaller channel spacing [5]–[7]. By using an on-chip interleaver, these limitations can be circumvented by dividing the comb into multiple buses, effectively halving the number of required resonators on a single bus while also doubling the channel spacing (Fig. 1(b)). Using the (de-)interleaver in this manner maintains compatibility with standard cascaded MRR architectures while mitigating inter-modulation crosstalk due to the increased channel spacing and additionally decreasing off-resonance IL since the number of MRRs in a given path is halved. Furthermore, this idea can be extended to multiple cascaded stages of (de-)interleavers in order to further sub-divide the comb, given that each successive stage has double the FSR of the previous.

Here, we demonstrate an ultra-broadband silicon photonic interleaver capable of interleaving and de-interleaving frequency comb lines over a 125 nm bandwidth from

Manuscript received October 8, 2020; revised December 5, 2020; accepted December 8, 2020. Date of publication December 11, 2020; date of current version December 21, 2020. This work was supported in part by the U.S. Advanced Research Projects Agency—Energy under ENLITENED Grant DE-AR000843 and in part by the U.S. Defense Advanced Research Projects Agency under PIPES Grant HR00111920014. The work of Anthony Rizzo was supported by the Department of Defense Science, Math, and Research for Transformation (SMART) Scholarship. *(Corresponding author: Anthony Rizzo.)*

Anthony Rizzo, Stuart Daudlin, and Keren Bergman are with the Lightwave Research Laboratory, Department of Electrical Engineering, Columbia University, New York, NY 10027 USA (e-mail: anthony.rizzo@columbia.edu).

Qixiang Cheng was with the Lightwave Research Laboratory, Department of Electrical Engineering, Columbia University, New York, NY 10027 USA. He is now with the Electrical Engineering Division, Department of Engineering, University of Cambridge, Cambridge CB3 0FA, U.K.

Color versions of one or more figures in this letter are available at https://doi.org/10.1109/LPT.2020.3044262.

Digital Object Identifier 10.1109/LPT.2020.3044262

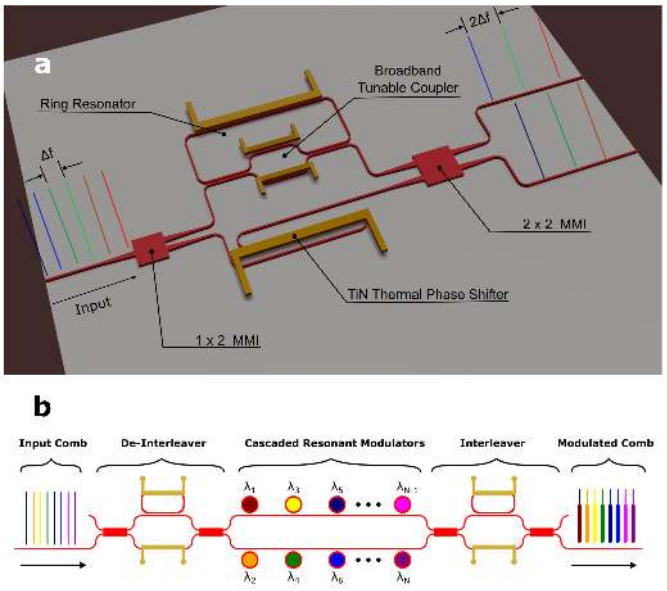

Fig. 1. (a) Device schematic and principle of operation, illustrating an incident frequency comb spectrum with line spacing Δf and two output groups each with spacing 2Δf. (b) Schematic of the proposed WDM link architecture using a single de-interleaver/interleaver pair to increase the channel spacing prior to modulation and then recombine the modulated channels into a single output.

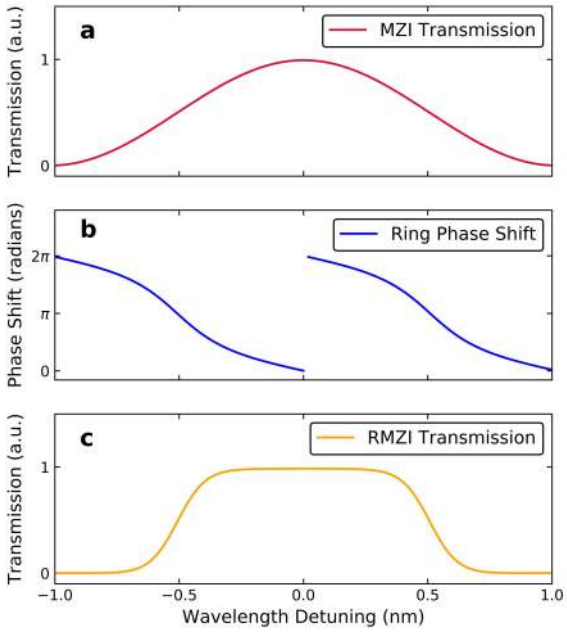

Fig. 2. (a) Single passband transmission for an asymmetric MZI as a function of detuning from the passband center. (b) Phase shift imparted by the resonator for the ideal coupling condition ($\kappa = 0.89$). (c) Output transmission for the RMZI system, demonstrating a flattened passband with sharper roll-off.

1525–1650 nm, spanning the full C- and L-bands. The device consists of a ring-assisted Mach Zehnder interferometer (RMZI) with broadband coupling to the ring, enabling consistent performance over the full bandwidth of interest. Previous demonstrations of silicon photonic interleavers have been restricted to usable spectral bandwidths less than 70 nm due to the use of standard directional couplers which are highly wavelength dependent [8], [9], and hybrid structures have required the use of an arrayed waveguide grating (AWG) for additional spectral selectivity which substantially increases the device footprint while also lacking flat-top passbands [10]. To the best of the authors' knowledge, this device represents the broadest operational bandwidth to date for an on-chip interleaver.

II. Device Design and Operating Principle

A. Fundamental Characteristics of RMZI Interleavers

RMZIs blend two of the fundamental building blocks of silicon photonics: micro-ring resonators (MRRs) and Mach Zehnder interferometers (MZIs). RMZIs have found use as wavelength-and-space selective switches [11], athermal MRRs [12], and wavelength interleavers [9], [13]. When operating as a wavelength interleaver, an input frequency comb with line spacing Δf is first incident on a 1×2 splitter which splits the power into the two MZI arms (Fig. 1). The top arm is coupled to a MRR while the bottom arm imparts a relative phase shift between the arms from the path length difference Δd. The two arms are then recombined on a 2×2 combiner and output in two groups, one with "even" wavelengths and one with "odd" wavelengths, both with line spacing 2Δf (Fig. 1). As a linear optical device, this operation is bidirectional, meaning that it can also be used to combine two separate frequency combs with spacing 2Δf into a single comb with spacing Δf assuming that the two combs are originally offset by Δf.

To achieve flat-top passbands compared to the sinusoidal passbands of a standard asymmetric MZI, the coupled MRR is used as a wavelength-selective phase shifter to alter the RMZI output at particular wavelengths. The free spectral range (FSR) of the MRR determines the periodicity of these phase shifts in the spectral domain, while the coupling coefficient (κ) determines the shape of the imparted phase as a function of detuning from resonance [15]. By aligning the resonances of the ring on the edges of the MZI passbands and choosing the proper value of κ, the phase response can flatten the MZI output to give a sharper, box-like spectral response (Fig. 2). The characteristic equations of the RMZI structure to achieve the proper spectral response for a particular FSR are given by

$$L_{ring} = \frac{2c}{n_g \mathrm{FSR}}, \tag{1}$$

$$\Delta \mathrm{d} = \frac{L_{ring}}{2} \tag{2}$$

where L_{ring} is the path length of the ring, Δd is the path length imbalance in the MZI arms, c is the speed of light in vacuum, n_g is the group index of the fundamental transverse electric (TE) mode, and FSR is the desired free spectral range. These relations hold assuming that the phase shift imparted by the MRR-MZI coupler is negligible (point coupler), but for couplers with longer interaction lengths, this phase must be included in the calculation of L_{ring} and Δd.

Figure 2 illustrates the principle of passband flattening for a single channel, with the ideal MRR-MZI coupling occuring at $\kappa = 0.89$ [9]. It is well known that standard evanescent-based directional couplers (DCs) are highly dispersive, meaning that

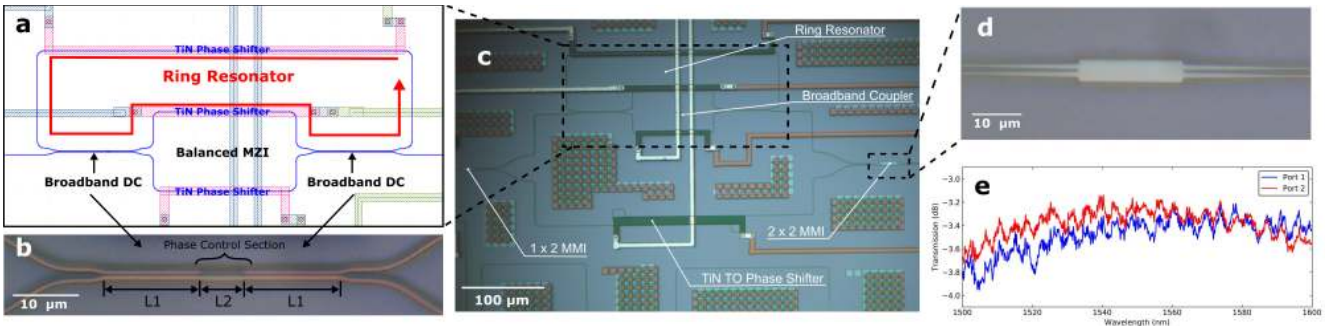

Fig. 3. (a) Layout of the broadband coupler to the ring, showing the path of the resonant cavity which contains the balanced MZI tunable coupler. (b) Broadband 50–50 coupler using a phase-control section, with L1 = 12.4μm and L2 = 4.6μm. For more details of the device structure, see [14]. (c) Optical microscope image of the fabricated device. (d) Optical microscope image of the 2 × 2 MMI. (e) Transmission spectrum of the MMI.

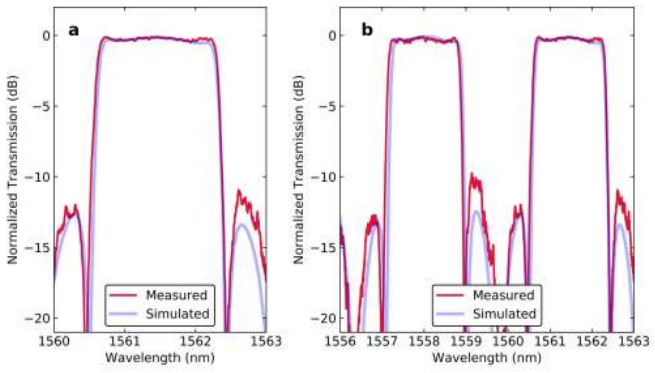

Fig. 4. Comparison of simulation with the experimentally measured device (after thermal tuning to correct for fabrication variations) for (a) single pass-band bandwidth and (b) free spectral range.

the coupling coefficient is a strong function of wavelength. For these standard DCs, it is clear that since κ varies with wavelength, the shape of the phase response will also vary with wavelength and thus the flat-top passbands will not be maintained over a wide bandwidth. Therefore, for broadband performance, it is critical to take great care in the design of the MRR-MZI coupler to ensure that: (i) the coupling coefficient is uniform across the bandwidth of interest, and (ii) the coupling coefficient is as close to the ideal value as possible such that the phase response at all wavelengths leads to the correct flattened passband shape.

B. Device Design and Simulation

The group index n_g for a 500 nm × 220 nm waveguide was simulated using a finite difference eigenmode solver (Lumerical MODE [16]) over the wavelength range of interest which was then used to calculate L_{ring} and Δd from Equations (1) and (2). The full device was then simulated using an S-parameter-based circuit simulator (Lumerical INTERCONNECT) to fine-tune L_{ring} and Δd to achieve the desired spectral response. This fine-tuning is necessary due to the fact that the phase shift imparted by the broadband coupler is determined by the effective index of the supermodes rather than the effective index of a standard 500 nm × 220 nm waveguide mode, which is not captured in Equations (1) and (2). However, this tuning can be done in a semi-automated way by first converting the lengths in Equations (1) and (2) into phase shifts for the standard waveguide dimensions, then using a 3D FDTD solver to calculate the effective phase shift imparted by the broadband coupler, subtracting this from the converted phases, and finally converting the phases back into waveguide length. This will yield adjusted values for L_{ring} and Δd which account for the phase shift imparted by the broadband coupler since the coupler is part of both the ring path and top MZI path. The broadband coupler was designed using a balanced MZI with phase-control-based 50-50 directional couplers as the splitters and combiners [14]. By using a balanced MZI design as the coupler rather than a fixed coupling element, the coupling coefficient can be tuned by adjusting the relative phase shift between the paths. The wavelength dependence and interferometric visibility of this device are determined by the splitter and combiner, which necessitates the use of broadband couplers for both of these elements. For the input and output broadband multi-mode interferometers (MMIs) of the RMZI, black-box process design kit (PDK) elements provided by the foundry were used. A microscope image and transmission spectrum of the 2 × 2 MMI are shown in Fig. 3(d) and 3(e), respectively. Since MMIs cannot be tuned post-fabrication to correct for variations, it is important that these devices be robust to the 3σ (99.7%) process corners for width and height variations in the particular foundry process used in order to ensure good yield. While a comprehensive analysis of the sensitivity of the MMI to fabrication variations is outside the scope of this work, it has been shown in the past that broadband device performance is a valid heuristic for robustness to fabrication variations [17] and steps can be taken at the design stage of the MMI to increase its tolerance to fabrication variations, such as choosing a larger body width [18].

III. Experimental Results

The device was fabricated through Advanced Micro Foundry's (AMF) 200 mm multi-project wafer (MPW) service. An optical microscope image of the fabricated device is shown in Fig. 3, demonstrating a compact device footprint of 200 μm × 800μm. The thermo-optic phase shifters were implemented using a titanium nitride layer as a resistive heater over the silicon waveguide layer. By snaking the waveguide under the heating element to maximize the overlap between

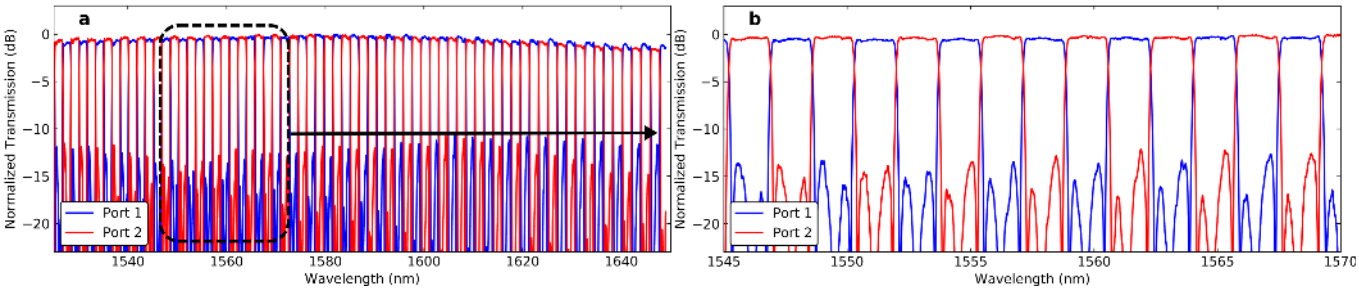

Fig. 5. (a) Experimentally measured spectrum of the tuned interleaver showing broadband performance over 125 nm of optical bandwidth from 1525–1650 nm. (b) Zoomed section of the spectrum from 1545–1570 nm showing the maintained flat-top response of the pass- and stop-bands.

the generated heat and the optical path, an ultra-efficient P_π of 14 mW ($V_\pi = 0.8$ V) was measured without the need for advanced fabrication techniques such as undercutting. Test structures of individual phase-control-based 3 dB couplers confirmed better than 1 dB of uniformity with minimal insertion loss over a 100 nm bandwidth. After tuning to correct for fabrication variations, the single passband bandwidth and FSR of the RMZI device very closely match the simulated design (Fig. 4). Furthermore, these properties are maintained over the full bandwidth of interest from 1525 – 1650 nm, demonstrating the uniform performance of the broadband MRR-MZI coupling (Fig. 5).

IV. Conclusion

We have demonstrated an ultra-broadband silicon photonic interleaver capable of interleaving and de-interleaving frequency comb lines over a 125 nm bandwidth, which represents a 55 nm improvement over previously reported devices [9]. The passbands exhibit an exceptionally uniform flat-top response, with a worst-case crosstalk suppression ratio of 10 dB over the full 125 nm and typical crosstalk suppression ratio around 15 dB. This key metric can be improved to $>$ 20 dB extinction through further optimization of the coupler to the ring. The envelope of the spectrum decays only 1.5 dB from the peak value between 1525–1650 nm, indicating that continued scaling in wavelength will not be insertion loss limited but rather dispersion and crosstalk limited. Through the use of advanced design techniques such as dispersion engineering for the waveguides and inverse design for the couplers, continued scaling to bandwidths over 150 nm with little to no degradation in performance appears possible. In addition to the primary use-case of optical communications, the demonstrated device is promising for any application that would benefit from on-chip processing of frequency combs, such as spectroscopy and metrology.

Acknowledgment

The authors thank Advanced Micro Foundry (AMF) for device fabrication and Hao Yang for helpful discussions.

References

[1] N. Jones, "The information factories," *Nature*, vol. 561, pp. 163–166, Sep. 2018.
[2] Q. Cheng, M. Bahadori, M. Glick, S. Rumley, and K. Bergman, "Recent advances in optical technologies for data centers: A review," *Optica*, vol. 5, no. 11, pp. 1354–1370, 2018.
[3] J. Pfeifle *et al.*, "Coherent terabit communications with microresonator kerr frequency combs," *Nature Photon.*, vol. 8, no. 5, pp. 375–380, May 2014.
[4] P. Marin-Palomo *et al.*, "Microresonator-based solitons for massively parallel coherent optical communications," *Nature*, vol. 546, no. 7657, pp. 274–279, Jun. 2017.
[5] Y. London *et al.*, "Performance requirements for terabit-class silicon photonic links based on cascaded microring resonators," *J. Lightw. Technol.*, vol. 38, no. 13, pp. 3469–3477, Jul. 1, 2020.
[6] Y. London *et al.*, "Energy efficiency analysis of comb source carrier-injection ring-based silicon photonic link," *IEEE J. Sel. Topics Quantum Electron.*, vol. 26, no. 2, pp. 1–13, Mar. 2020.
[7] A. Rizzo, L. Y. Dai, X. Meng, Y. London, J. Patel, M. Glick, and K. Bergman, "Ultra-low power consumption silicon photonic link design analysis in the AIM PDK," *Proc. SPIE*, vol. 10924, pp. 31–36, Mar. 2019.
[8] X. Jiang *et al.*, "Design and experimental demonstration of a compact silicon photonic interleaver based on an interfering loop with wide spectral range," *J. Lightw. Technol.*, vol. 35, no. 17, pp. 3765–3771, Sep. 1, 2017.
[9] L.-W. Luo *et al.*, "High bandwidth on-chip silicon photonic interleaver," *Opt. Exp.*, vol. 18, no. 22, pp. 23079–23087, Oct. 2010.
[10] D. Dai, "Multi-channel wavelength/mode-division-multiplexers on silicon," in *Proc. Optical Fiber Commun. Conf.*, Washington, DC, USA: United Optical Society of America, 2016, pp. 1–3.
[11] Y. Huang, Q. Cheng, A. Rizzo, and K. Bergman, "Push—pull microring-assisted space-and-wavelength selective switch," *Opt. Lett.*, vol. 45, no. 10, pp. 2696–2699, May 2020.
[12] B. Guha, B. B. C. Kyotoku, and M. Lipson, "Cmos-compatible athermal silicon microring resonators," *Opt. Exp.*, vol. 18, no. 4, pp. 3487–3493, Feb. 2010.
[13] A. Rizzo, Q. Cheng, S. Daudlin, and K. Bergman, "Ultra-broadband silicon photonic interleaver for massive channel count frequency combs," in *Proc. Conf. Lasers Electro-Optics*, 2020, pp. 1–2.
[14] Z. Lu *et al.*, "Broadband silicon photonic directional coupler using asymmetric-waveguide based phase control," *Opt. Exp.*, vol. 23, no. 3, pp. 3795–3808, Feb. 2015.
[15] W. Bogaerts *et al.*, "Silicon microring resonators," *Laser Photon. Rev.*, vol. 6, no. 1, pp. 47–73, Jan. 2012.
[16] *Accurately Simulate Photonic Components and Circuits*. Accessed: Oct. 6, 2020. [Online]. Available: https://www.lumerical.com/products
[17] J. Lu and J. Vučković, "Nanophotonic computational design," *Opt. Exp.*, vol. 21, no. 11, pp. 13351–13367, Jun. 2013.
[18] Z. Sheng *et al.*, "A compact and low-loss MMI coupler fabricated with CMOS technology," *IEEE Photon. J.*, vol. 4, no. 6, pp. 2272–2277, Dec. 2012.